Electronic Supplementary Material (ESI) for Journal of Materials Chemistry A.
This journal is © The Royal Society of Chemistry 2024

Nanoscale Stirring at Liquid-Liquid Interface: Interfacial Nano-Vortexer Actively Converges Immiscible Biphasic Reactants for Enhanced Phase-Transfer Catalysis

Zhi Zhong Ang [a], Veronica Pereira [a], Siew Kheng Boong [a], Haitao Li [b], and Hiang Kwee Lee* [a] [c] [d]

[a] Division of Chemistry and Biological Chemistry, School of Chemistry, Chemical Engineering and Biotechnology, Nanyang Technological University, 21 Nanyang Link, Singapore 637371 (Singapore)

[b] School of Chemistry and Chemical Engineering, Yangzhou University, Yangzhou, 25002 (P. R. China)

[c] Institute of Materials Research and Engineering, The Agency for Science, Technology and Research (A*STAR), 2 Fusionopolis Way, #08-03, Innovis, Singapore 138634 (Singapore)

[d] Centre for Hydrogen Innovations, National University of Singapore, E8, 1 Engineering Drive 3, Singapore 117580 (Singapore)

*Correspondence to: hiangkwee@ntu.edu.sg

Experimental Section

Chemicals

[3-(N,N-dimethylamino)propyl]trimethoxysilane (> 96%) was purchased from Tokyo Chemical Industry (TCI). Iron (II, III) oxide powder (Fe_3O_4, 95 %), tetraethyl orthosilicate (TEOS, 98 %), ammonium hydroxide solution (28–30 %, ACS reagent), phenol (≥ 99%, purified by redistillation), tetrabutylammonium bromide (ACS reagent, 98%), bromothymol blue (dye content, ≥ 95 %) and decane (≥ 95%) were purchased from Sigma-Aldrich. Nitric acid (HNO_3, 69 %) was from Honeywell Research Chemicals. Ethyl acetate (≥ 99.8 %,), acetone (≥ 99.8 %), hexanes (HPLC grade), and 2-propanol (≥ 99.5 %) were purchased from Thermo Fisher Scientific. All chemicals were used without further purification. Milli-Q water (> 18.0 MΩ.cm) was purified with a Sartorius Arium 611 ® UV ultrapure water system.

Synthesis of Fe_3O_4@SiO_2 nanochains

Commercial Fe_3O_4 powders were first washed with ample amounts of organic solvents (e.g. ethanol, acetone, hexanes, and 2-propanol) to remove any capping agents that could be present on their surfaces. The washed Fe_3O_4 powders were subsequently re-dispersed in 2-propanol at a concentration of ~1.5 mg/mL. 1 mL of the Fe_3O_4 suspension was added into a 20 mL reaction vial containing 0.2 mL of TEOS and 5.8 mL of 2-propanol. After which, 1.5 mL of water and 1.5 mL of ammonium hydroxide solution (1.11 M) in 2-propanol were added to the reaction mixture. The reaction solution was quickly homogenized using commercial vortex shaker and immediately placed between two sets of permanent magnets to suspend and align magnetic Fe_3O_4 nanoparticles into chain-like structures. The silica coating process was left to react for 30 min. As-synthesized

Fe_3O_4@SiO_2 nanochains were then washed with ample ethanol, and subsequently re-dispersed and stored in ethanol (3 mg/mL).

Functionalization of Fe_3O_4@SiO_2 nanochains

5 mL of the ethanolic suspension containing Fe_3O_4@SiO_2 nanochains was first treated with 30 µL of [3-(N,N-Dimethylamino)propyl]trimethoxysilane followed by 30 µL of water. The mixture was stirred at 1000 rpm for 3 days. The functionalized Fe_3O_4@SiO_2 nanochains were then washed with ample ethanol, and subsequently redispersed and stored in ethanol (3 mg/mL).

Characterization of the spinning dynamics of Fe_3O_4@SiO_2-based interfacial nano-vortexers

Approximately 0.3 mL of the ethanolic suspension containing Fe_3O_4@SiO_2 nanochains was washed with either decane or water before being dispensed onto a silicon substrate. The platform was then placed on top of a commercial magnetic stirrer. It is noteworthy that the nanochains settled on the silicon substrate instead of suspending in the solution due to their large particle size and correspondingly stronger magnetic properties. The settling of nanochains on the Si substrate is crucial to facilitate the facile observation of their spinning behavior via an optical microscope. The spinning of the nanorod was then initiated using an applied magnetic field rotating at 100 – 1100 rpm as conveyed by a commercial magnetic stirrer. The spinning process of the nanochains was tracked and recorded using a high-speed camera (~35 fps) that was mounted on an optical microscope. The recorded video was then analyzed frame by frame to determine the time required for the nanochain to complete one revolution along its own axis. The corresponding spin rate of the nanochain was then calculated using this information.

Investigation on the effect of spinning interfacial nano-vortexer on bulk solutions

0.84 mL of the ethanolic suspension containing interfacial nano-vortexers was washed with ethyl acetate and redispersed in 0.6 mL of ethyl acetate. 75 μL of this suspension was added to 0.3 mL of bromothymol blue (BTB) dye solution in ethyl acetate (1.25 mM). 0.25 ml of this suspension was then placed on top of 0.5 mL of aqueous NaOH solution (1 M). The spinning of the interfacial nano-vortexer was initiated by applying a rotating magnetic field (0 – 1100 rpm) conveyed using a commercial magnetic stirrer. The effects of spinning interfacial nano-vortexers on the two immiscible bulk solutions were captured with a high-speed optical camera at 240 fps. The optical images were processed using ImageJ and the images' red channel was analyzed. The red channel intensity was used to trace a continuous travel path of BTB probe molecules in the aqueous phase.

Quantification of phenol, 2-nitrophenol and 4-nitrophenol using UV-visible absorption spectroscopy

A calibration curve relating absorption intensity of either 2-nitrophenol (2-NP) and 4-nitrophenol (4-NP) concentration was first established for subsequent quantification in the reaction solution. The individual nitrophenol was first dissolved in ethyl acetate and further serial-diluted to various concentration between 0.04 M and 0.2 M. The individual nitrophenol standard solution was first diluted by a dilution factor of 2000. The solutions were measured using UV-visible absorption spectroscopy. The characteristic peaks at 305 nm and 349 nm were used for the quantification of 4-NP and 2-NP, respectively.

As the nitration reaction produced a mixture of 2-NP and 4-NP, each type of nitrophenol was quantified through a two-step calibration process which first identified the ratio between the two

products. This was followed by the subsequent determination of the concentration of each product. See Figure S11 and Supplementary Information 1 for more details.

For phenol quantification, a calibration curve relating the absorption intensity with its concentration was first established for subsequent quantification in the solution. Phenol was first dissolved in ethyl acetate and further serial-diluted to various concentration between 0.02 M and 0.1 M. The individual phenol standard solution was diluted by a dilution factor of 1000. The absorption spectra were measured using UV-visible absorption spectroscopy and subsequently used for phenol quantification using its characteristic peak at 269 nm.

Phase-transfer catalysis for the biphasic nitration reaction using interfacial nano-vortexers

0.84 mL of the nano-vortexers suspension in ethanol was washed and re-dispersed in 0.6 mL of ethyl acetate. 75 µL of this suspension was added to 0.3 mL of ethyl acetate (i.e., the organic phase) containing phenol reactant (0.25 M) and Bu_4NBr (0.025 M) as the phase-transfer catalyst. 0.25 ml of this phenolic suspension (0.21 mg of the nano-vortexers) was then positioned onto 0.5 mL of aqueous HNO_3 solution (6 wt%) functioning as a mild nitration agent. The reaction setup was then left standing for 1 min on the commercial magnetic stirrer for the nano-vortexers to assemble at the liquid-liquid interface between the immiscible aqueous solution and ethyl acetate. The biphasic reaction was initiated under applied magnetic field rotating (100 - 1100 rpm) for 2 h. After the reaction, the interfacial nano-vortexers were removed using a permanent magnet and the organic phase (ethyl acetate) was analyzed using UV-visible absorption spectroscopy to determine the concentrations of various nitrophenols.

For experiments involving twin stirring, the same procedure was employed with the use of an additional commercial stirbar in the bottom aqueous phase.

Characterization

Scanning electron microscopy (SEM) images were collected on a JEOL-JSM-7600F microscope operated at 5kV. Attenuated total reflectance Fourier-transform infrared (ATR-FTIR) spectroscopy measurements were performed on a PerkinElmer Spectrum 100 FT-IR Spectrometer. A Canon PowerShot G7 X Mark III camera was used to capture the slow-motion video (240 fps). UV−visible absorption measurements were conducted using an AvaSpec-ULS2048CL-EVO-UA-50 equipped with a halogen light source (AvaLight-DH-S).

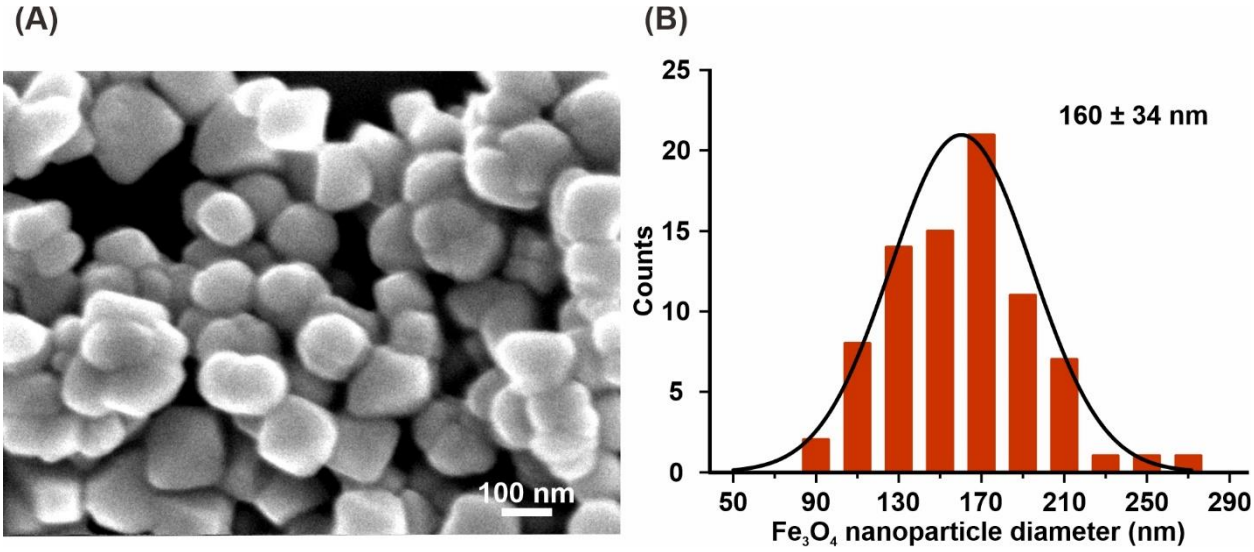

Figure S1. (A) SEM image and the corresponding (B) size distribution of Fe_3O_4 nanoparticles.

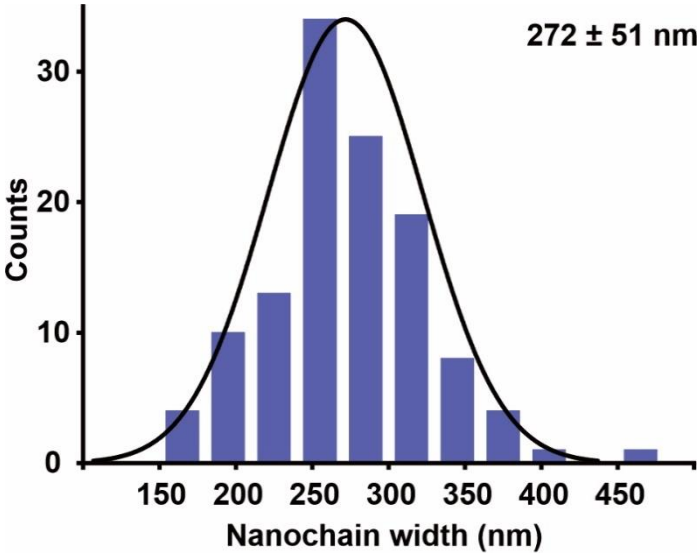

Figure S2. Width distribution of as-synthesized Fe_3O_4@SiO_2 nanochains.

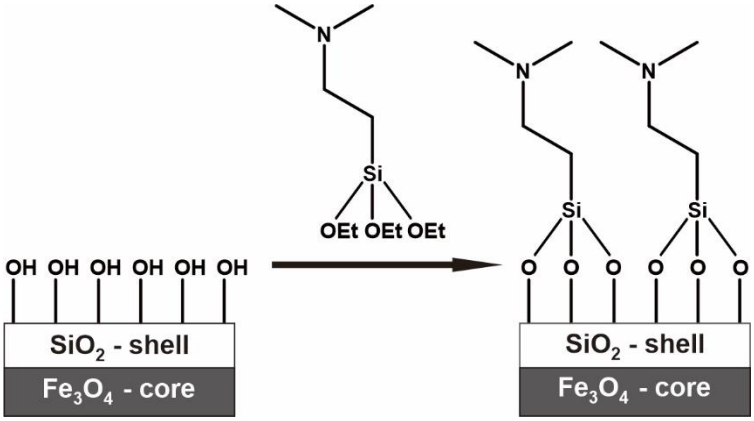

Figure S3. Surface functionalization of Fe_3O_4@SiO_2 nanochain.

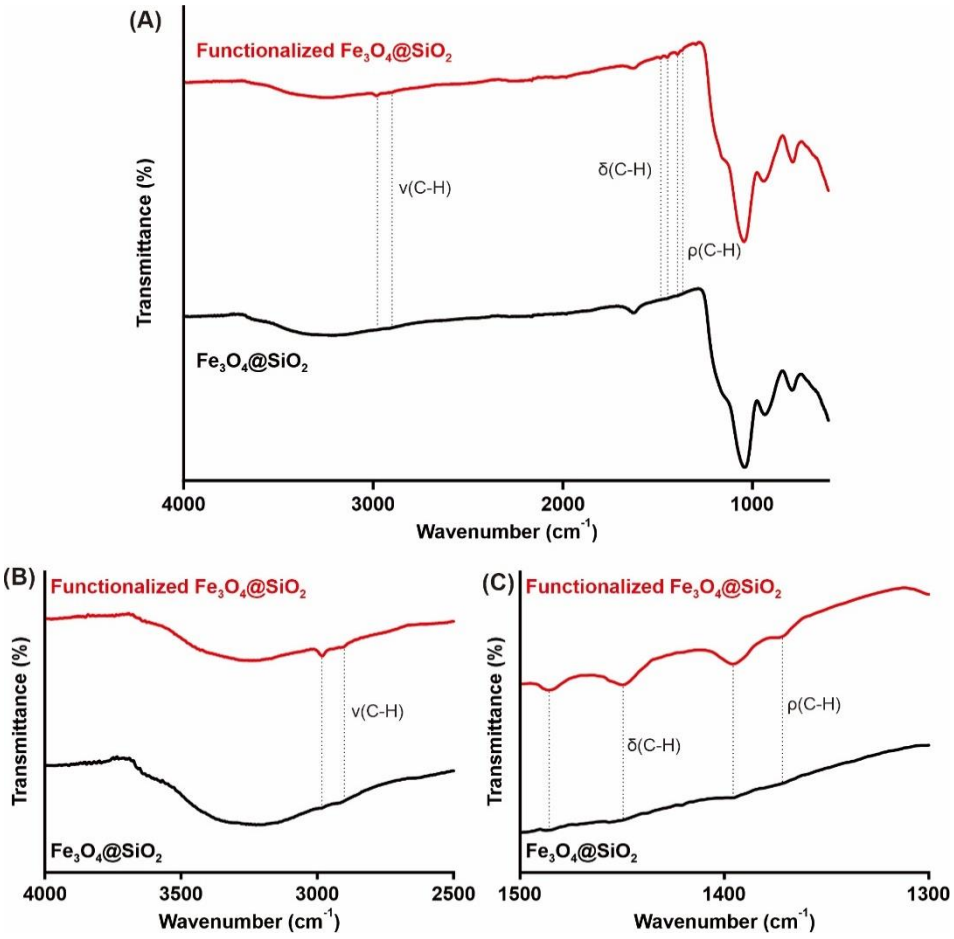

Figure S4: ATR-IR spectra of as-synthesized and functionalized Fe_3O_4@SiO_2 nanochains for wavenumber regions between (A) 700 – 4000 cm^{-1}, (B) 2500 – 4000 cm^{-1}, and (C) 1300 – 1500 cm^{-1}.

When compared to non-functionalized Fe_3O_4@SiO_2 nanochains, we note that the surface-functionalized platform exhibits two new vibrational modes at 2982 and 2912 cm^{-1} (Figure S4B) that are assigned to be the C-H stretching of the aminosilane. Furthermore, another 2 sets of vibrational features are also observed which can be assigned to the aminosilane's C-H bending vibration (1486 and 1450 cm^{-1}) and C-H rocking vibration (1396 and 1374 cm^{-1}).

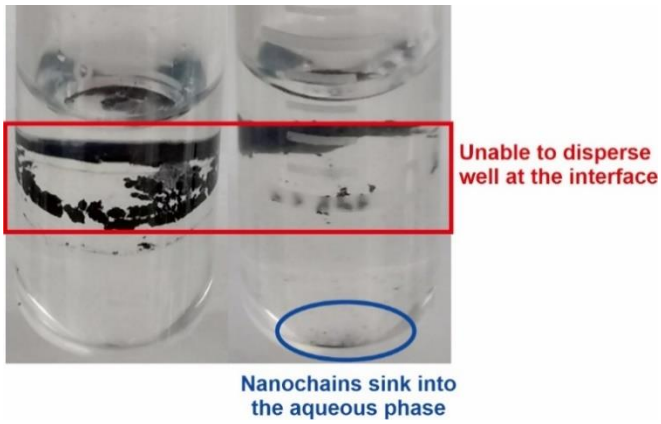

Figure S5. Unstable assembly of unfunctionalized Fe_3O_4@SiO_2 nanochains at the liquid-liquid interface formed between immiscible ethyl acetate and water.

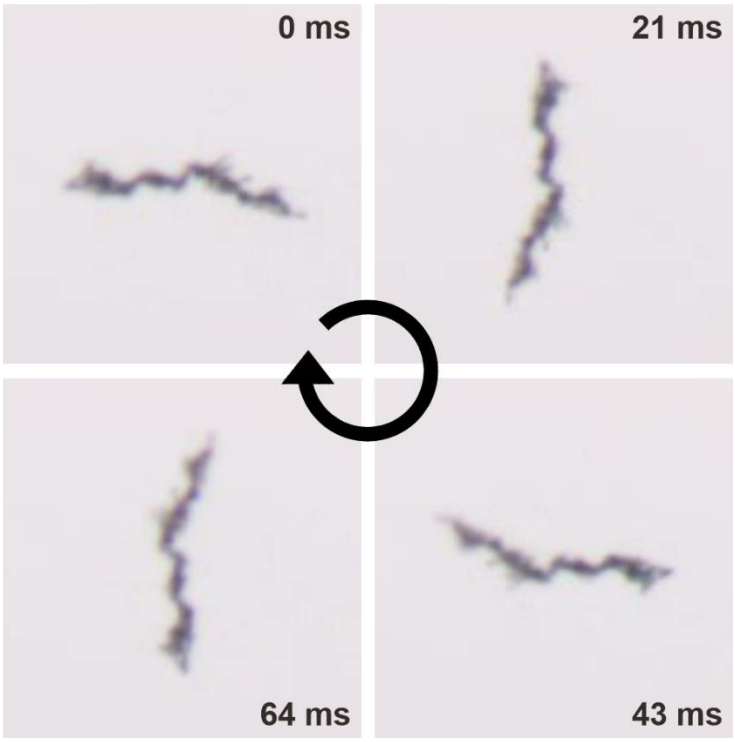

Figure S6. Digital snapshots showing the spinning motion of interfacial nano-vortexer at 700 rpm.

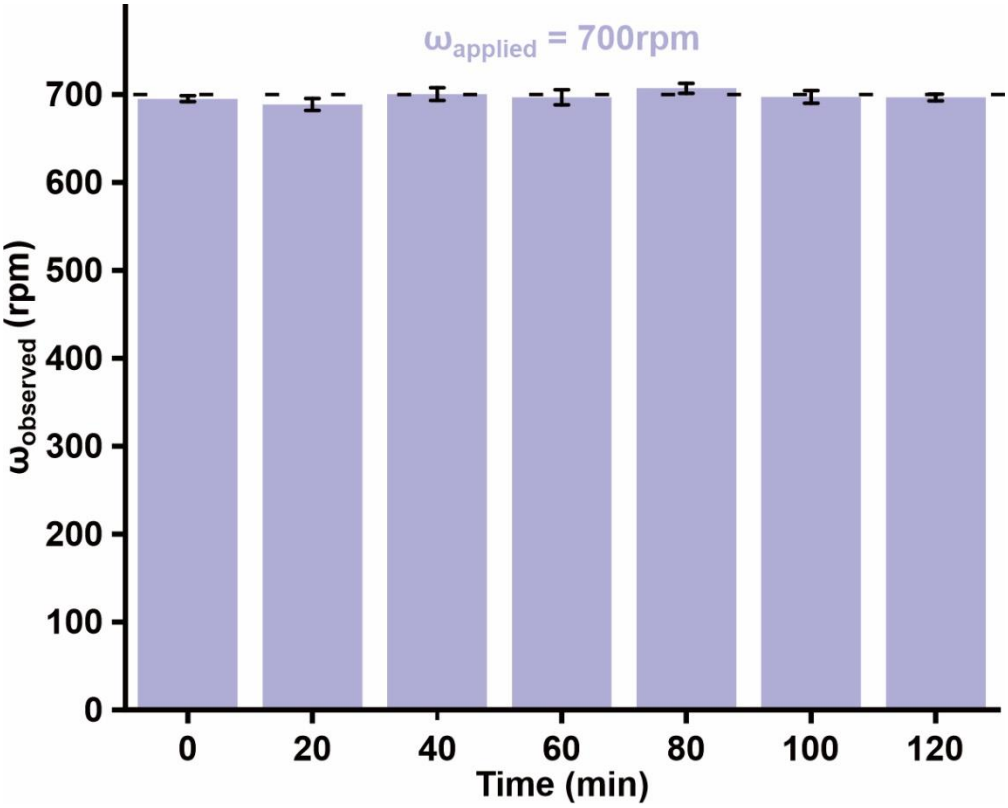

Figure S7. Evaluation of surface-functionalized Fe_3O_4@SiO_2 nanochains' spin rate over 2 hours when subjected to an applied magnetic field rotating at 700 rpm.

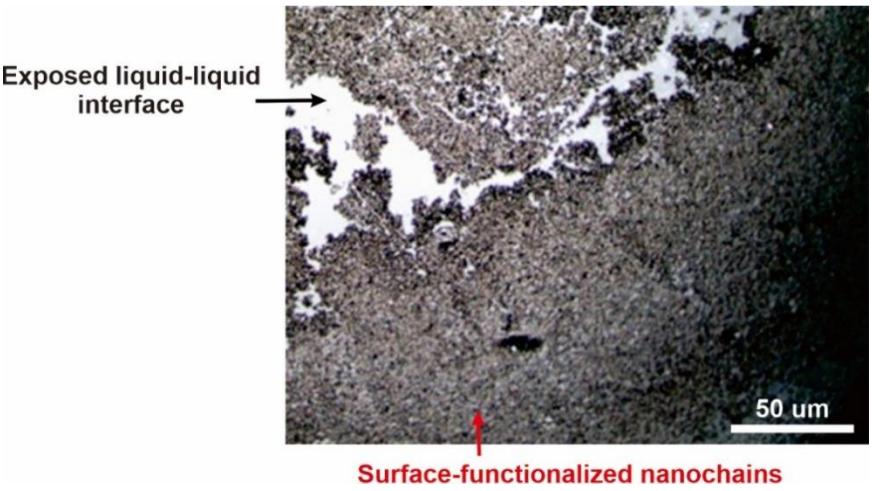

Figure S8. Microscopic image of the assembly of surface-functionalized Fe_3O_4@SiO_2 nanochains at the water-ethyl acetate interface.

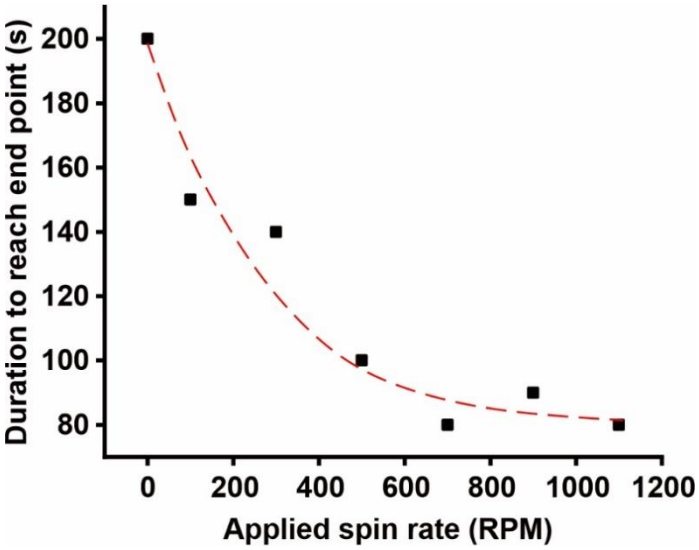

Figure S9. Duration for the bromothymol blue dye tracer to reach the target end point when in the presence of interfacial nano-vortexer spinning at 0 – 1100 rpm.

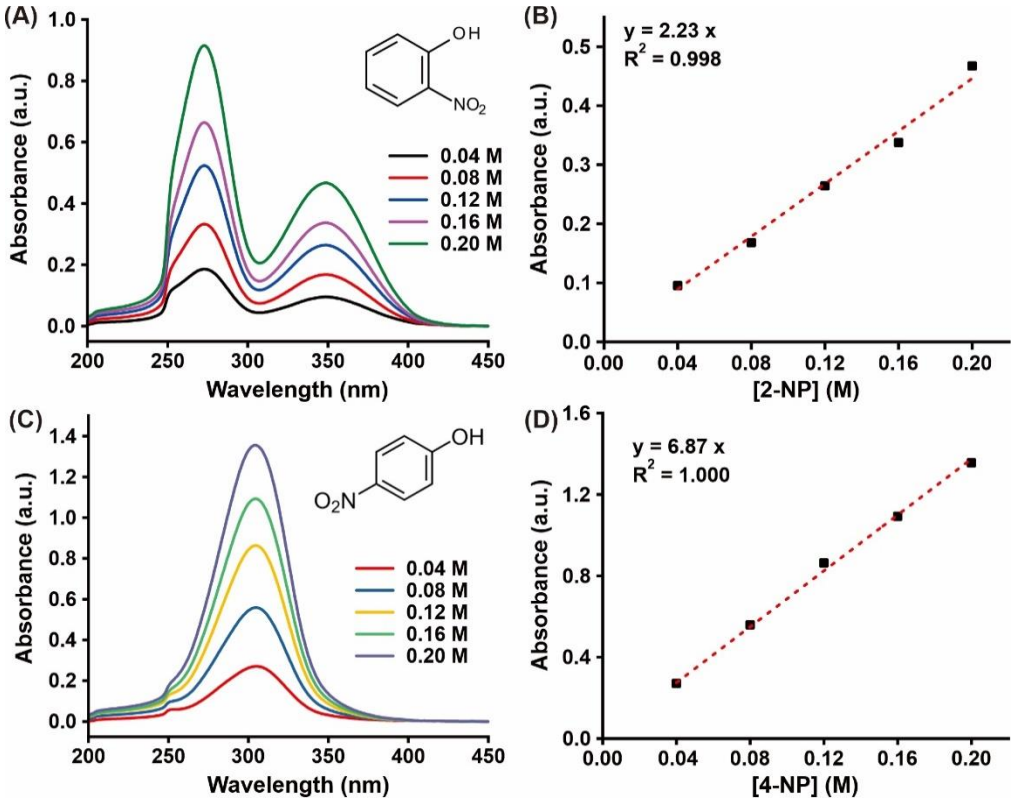

Figure S10. (A) UV-visible absorption spectra and the (B) corresponding calibration curve of 2-nitrophenol at different concentrations. (C) UV-visible absorption spectra and the (D) corresponding calibration curve of 4-nitrophenol at different concentrations.

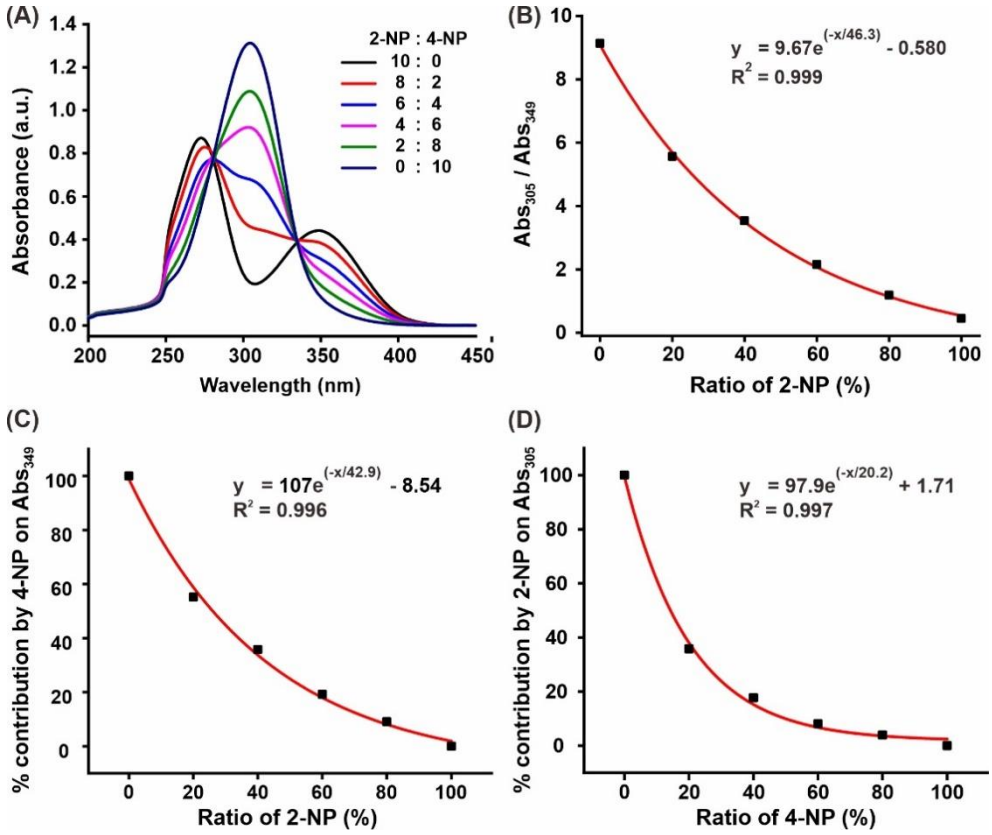

Figure S11. (A) UV-visible absorption spectra of a solution mixture of 2-nitrophenol and 4-nitrophenol in ethyl acetate at different ratio. (B) Calibration curve involving the ratio of absorbance at 305 nm vs 349 nm against the composition of 2-nitrophenol in the solution. (C) Contribution of 4-nitrophenol (4-NP) to the absorbance at 349 nm across various 2-nitrophenol (2-NP) composition. (D) Contribution of 2-NP to the absorbance at 305 nm across various 4-NP composition. For (C) and (D), the total concentration of nitrophenols is kept at 0.2 M.

Supplementary 1: Determination of 2-nitrophenol and 4-nitrophenol product concentrations from the nitration reaction.

We employ an alternative method to determine the concentration of various nitrophenol products owing to the overlap between their absorption spectra. Briefly, we prepare standard solutions containing pre-defined ratio of 2-nitrophenol and 4-nitrophenol and analyzed them through UV-visible absorption spectroscopy (Figure S11A). We subsequently compare the absorbance at 305 nm (mainly by 4-nitrophenol) and 349 nm (mainly by 2-nitrophenol) and establish a relationship as follows (Figure 11B):

$$\frac{\mathrm{Abs}_{305}}{\mathrm{Abs}_{349}} = 9.67\mathrm{e}^{\left(-\frac{x}{46.3}\right)} - 0.580 \qquad \text{---(1)}$$

where x is the composition of 2-nitrophenol (%).

By comparing the absorbance values (for 305 nm and 349 nm) in each mixture, we can exclude the contribution to absorbance values (Figure S11C, D) by the other nitrophenol species and accurately determine the actual absorbance arising from target nitrophenol species. These absorbance values are then compared against the calibration curves of individual nitrophenol species (Figure 10B, D) to calculate the concentrations of 2-nitrophenol and 4-nitrophenol present.

<u>Using a UV-visible absorption spectrum with the following peak absorbances as an example,</u>

Abs_{305} = 0.61546

Abs_{349} = 0.25323

Using equation (1),

$$x = -46.3 * \ln\left(\left(\frac{0.61546}{0.25323} + 0.580\right)/9.67\right)$$

x = 54.0%

This indicates that the solution contains 54% 2-nitrophenol and 46.0% 4-nitrophenol. Applying this to the calibration curves in Figure S11C, D:

For 2-nitrophenol:

$$y = 107\mathrm{e}^{\left(-\frac{54.0}{42.9}\right)} - 8.54$$

y = 21.8 %

For 4-nitrophenol:

$$y = 97.8\mathrm{e}^{\left(-\frac{46.0}{20.2}\right)} + 1.71$$

y = 11.7 %

Actual absorbance of target nitrophenol species after subtracting the contribution from the other nitrophenol species:

Abs_{305} = 0.61546 × (100 – 11.7)%

= 0.54345

Abs_{349} = 0.25323 × (100 – 21.8)%

= 0.19803

By comparing the representative absorbance of individual nitrophenol species to their calibration curves (Figure S10B, D):

[2-NP] = 0.19803 / 2.23

= 0.0888 M

[4-NP] = 0. 54345 / 6.87

= 0.0791 M

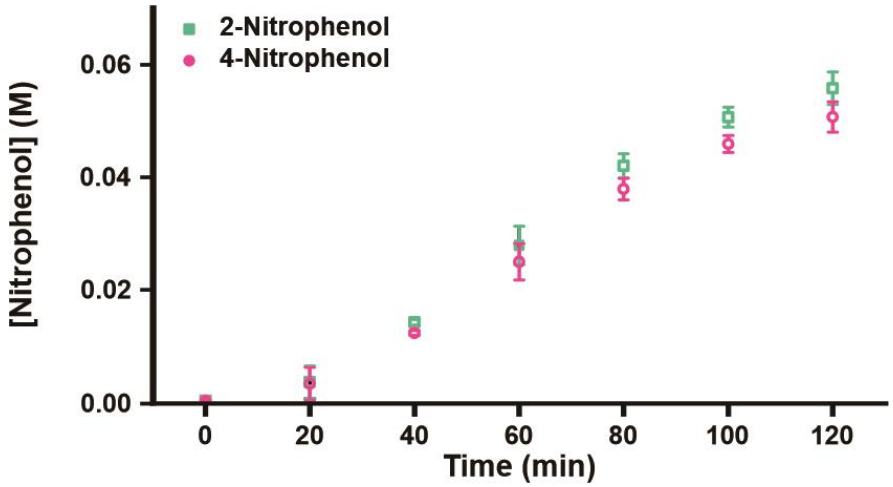

Figure S12. Time-dependent plot showing the concentrations of 2-nitrophenol and 4-nitrophenol produced during the nitration reaction in the presence of interfacial nano-vortexer.

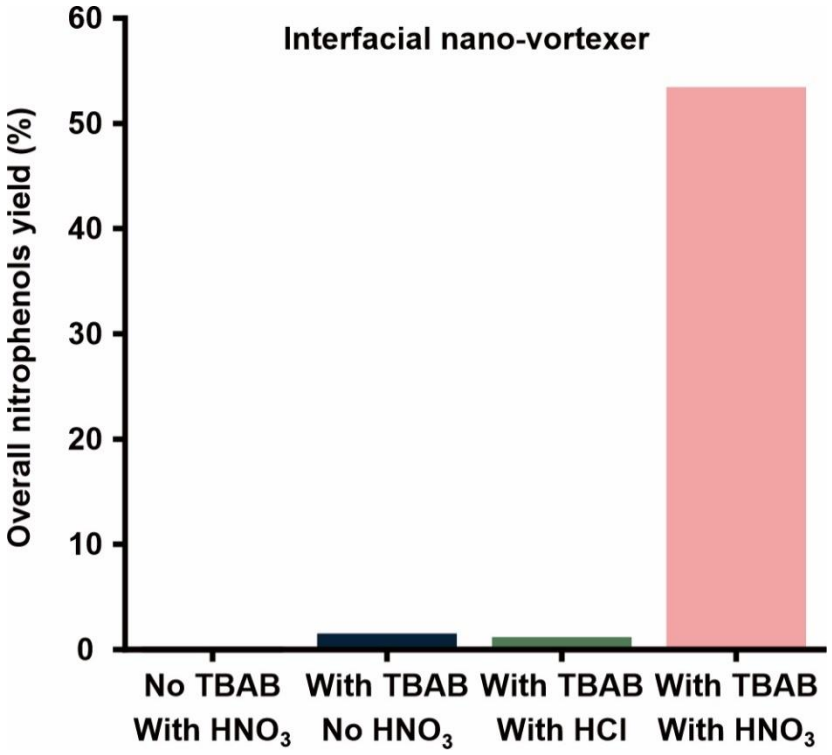

Figure S13. Overall nitrophenols yield obtained from the interfacial nitration reaction using interfacial nano-vortexer under various reaction conditions.

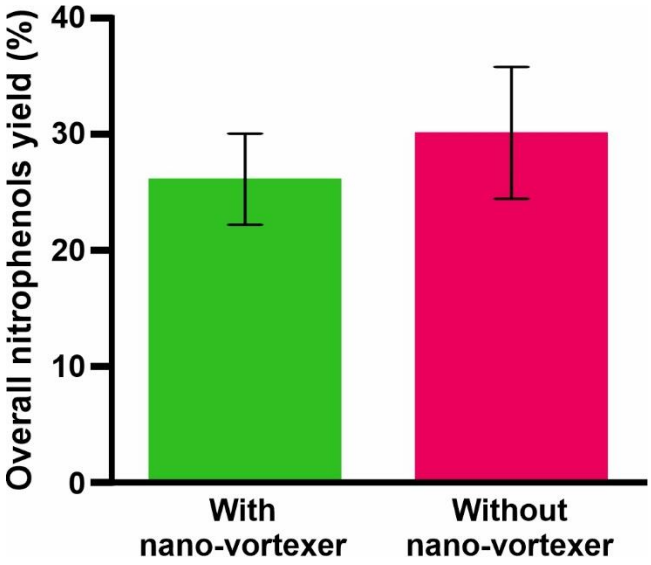

Figure S14. Yield of nitrophenol under static conditions (0 rpm) with and without loading of nano-vortexer.

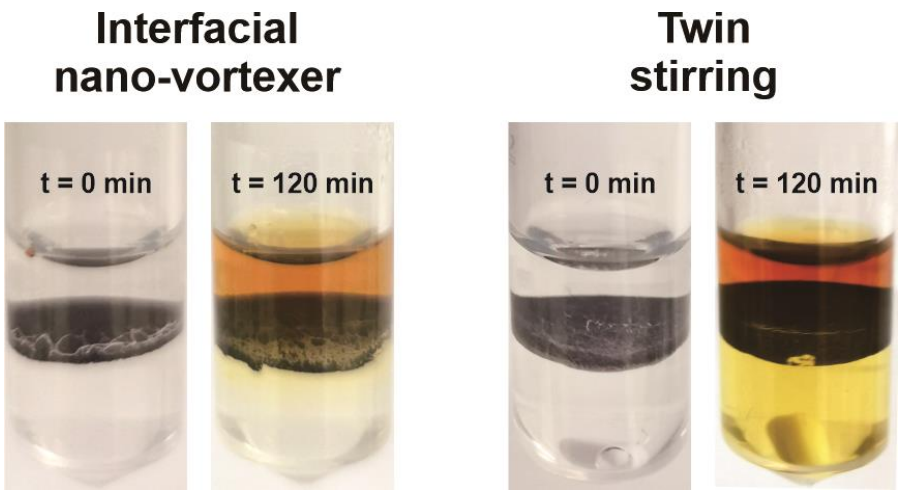

Figure S15. Optical images showing the biphasic reaction set-up before and after the nitration reaction when employing different mass manipulation methods.

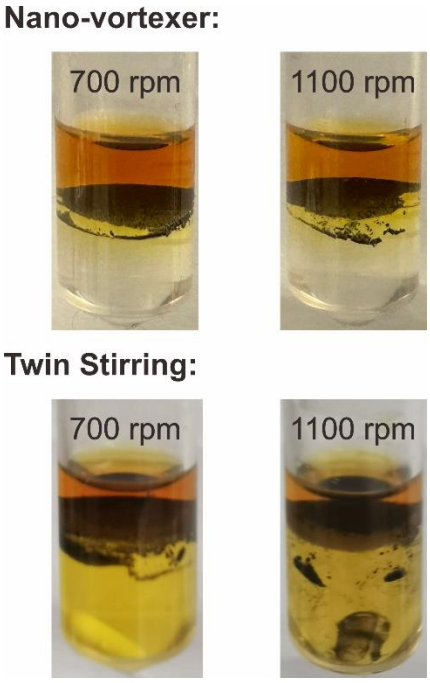

Figure S16. Dispersion of the nano-vortexer with and without commercial stirbar at different spin rates of 700 rpm and 1100 rpm.

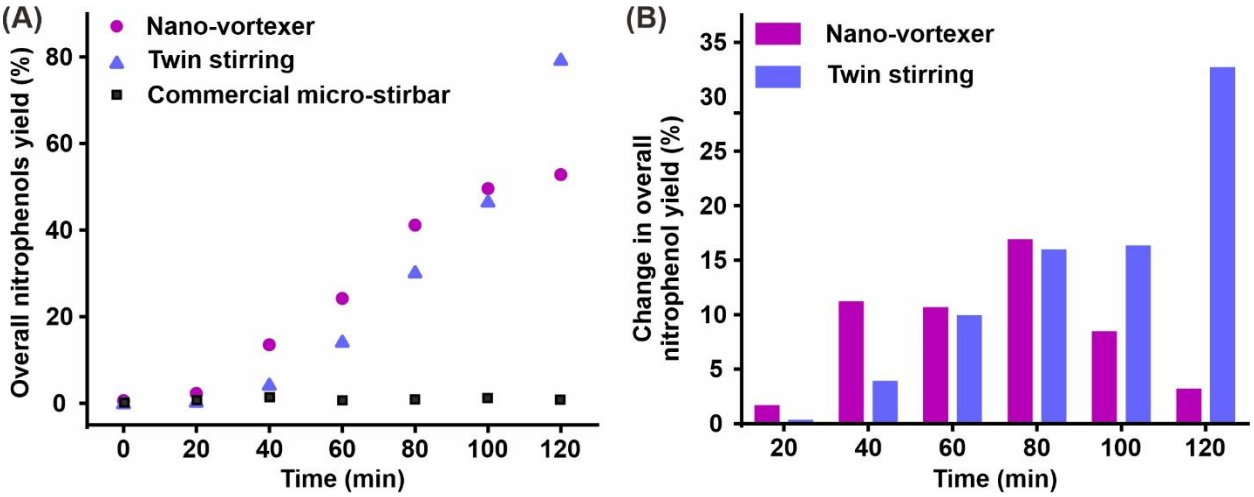

Figure S17. (A) Time-dependent monitoring of the overall nitrophenols yield when subjected to different mass manipulation methods at 700 rpm. (B) Corresponding change in overall nitrophenols yield at different time intervals.

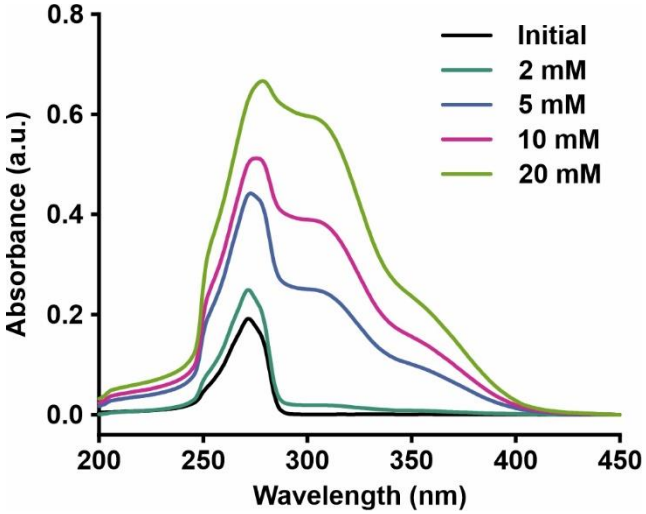

Figure S18. UV-visible absorption spectra of the ethyl acetate organic phase after the nitration reaction (time, 120 min) at various TBAB concentrations and in the presence of twin stirring.

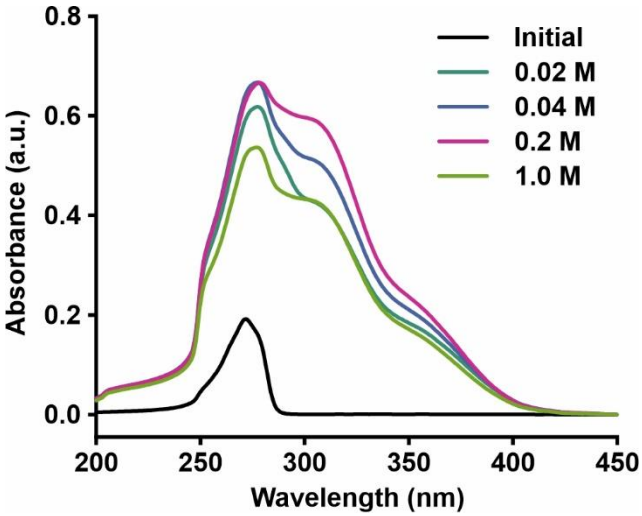

Figure S19. UV-visible absorption spectra of the ethyl acetate organic phase after the nitration reaction (time, 120 min) at various phenol concentrations and in the presence of twin stirring.

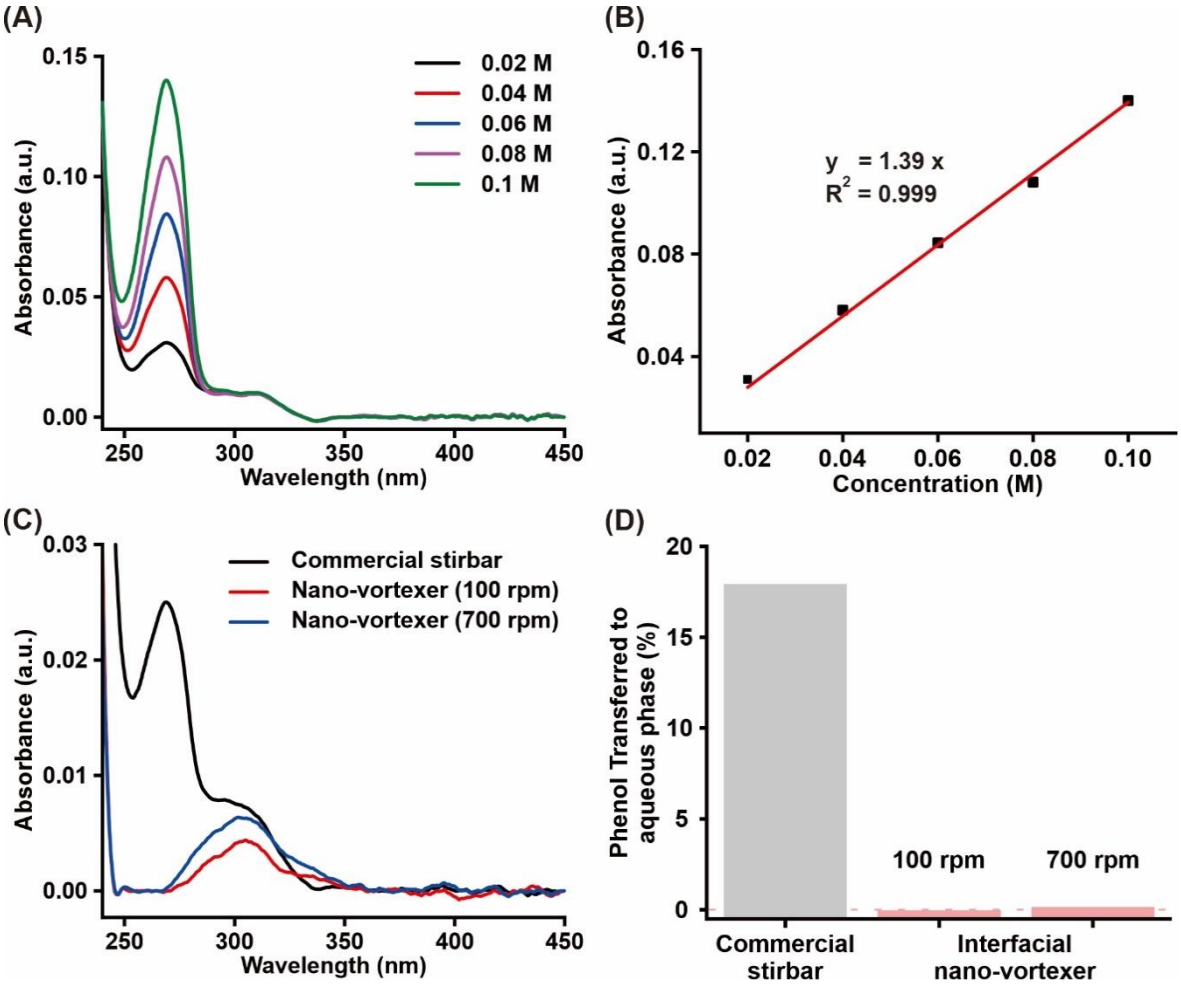

Figure S20. (A) UV-visible absorption spectra and the (B) corresponding calibration curve of phenol in 6% nitric acid at different concentrations. (C) UV-visible absorption spectrum of the nitric acid phase after nitration reaction using commercial stirbar or interfacial nano-vortexer for 120 mins. (D) Percentage of phenol transfer from the organic reaction phase to the aqueous non-reaction phase.

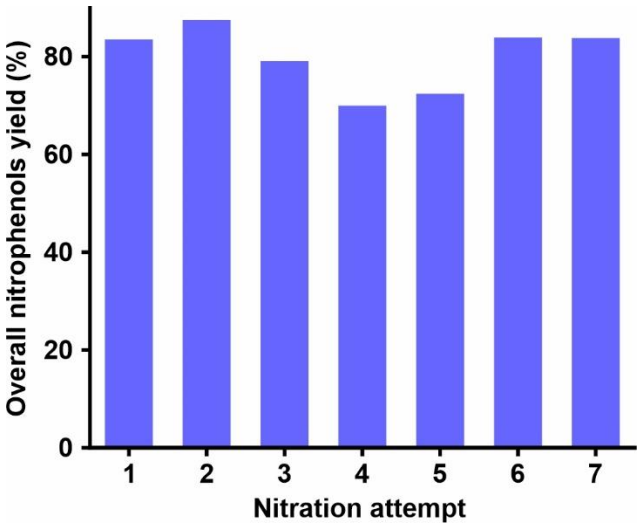

Figure S21. Reusability of the interfacial nano-vortexer across seven successive cycles of the phase-transfer catalysis.

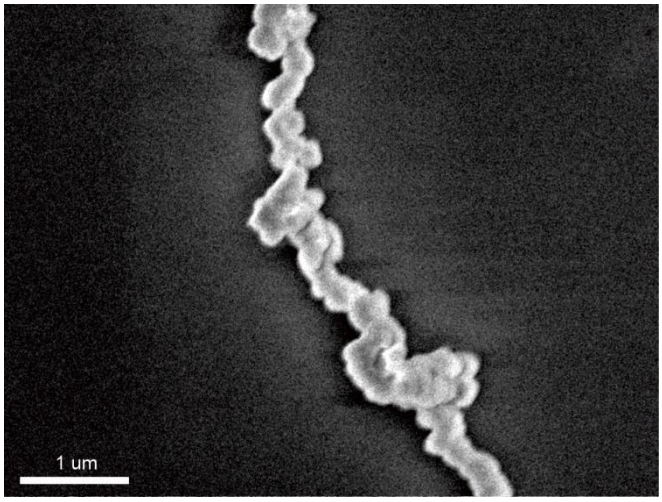

Figure S22. SEM image of the Fe_3O_4@SiO_2 nanochain after the phase-transfer catalysis.

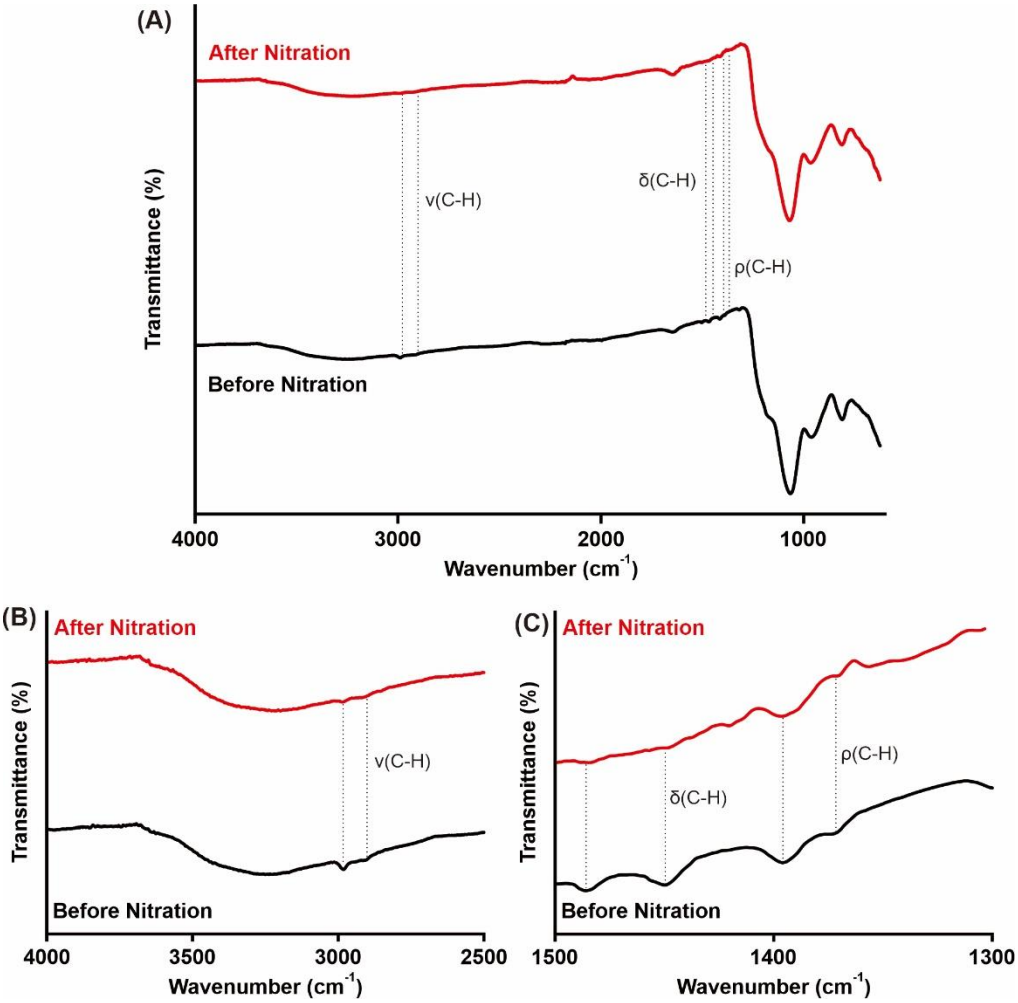

Figure S23. ATR-IR spectra of the functionalized Fe_3O_4@SiO_2 nanochains before and after the interfacial nitration reaction for wavenumber regions between (A) 700 – 4000 cm^{-1}, (B) 2500 – 4000 cm^{-1}, and (C) 1300 – 1500 cm^{-1}.